FEM ANALYSIS ON COLLAPSE OF UAV FROM DIFFERENT HEIGHTS

Gabriel Gheorghe[1], Iuliana Gageanu[1], Catalin Persu[1], Dan Cujbescu[1], Gheorghe Voicu[2]
[1]National Institute of Research-Development for Machines and Installations Designed to Agriculture and Food Industry, Romania; [2]University Politehnica of Bucharest, Romania
gabrielvalentinghe@yahoo.com, iulia.gageanu@gmail.com, persucatalin@yahoo.com, dcujbescu@yahoo.com, ghvoicu_2005@yahoo.com

Abstract. The FEM analysis in SolidWorks Simulation will present the study of drop tests evaluating the effect of the impact of a part or an assembly with a rigid or flexible planar surface. The program calculates impact and gravity loads automatically. No other loads or restraints are allowed. The program solves a dynamic problem as a function of time. The general equation of motion is: $FI(t) + FD(t) + FE(t) = R(t)$, where $FI(t)$ are the inertia forces, $FD(t)$ are the damping forces, and $FE(t)$ are the elastic forces. All of these forces are time-dependent. Increased requirements for reliability and safety, included in contemporary standards and norms, have a high impact over new product development. New numerical techniques based on virtual prototyping technology facilitate improving the product development cycle, resulting in reduced time·m^{-1}oney spent for this stage, as well as increased knowledge about certain failure mechanisms. The so-called "drop test" has become nearly a "must" step in the development of any human operated product. This study aims to demonstrate the dynamic behaviour assessment of a structure under impact loads, based on virtual prototyping using a typical nonlinear analysis – explicit dynamics. Different height and drop orientations were analyzed and critical load cases and design weaknesses have been found. Design modifications have been proposed, based on detailed analyses results review.

Keywords: UAV, drop test, von Mises Stress, equivalent strain.

Introduction

The use of unmanned aerial vehicles (UAVs) in a wide variety of fields allows successful performance of various tasks. UAVs allow their use in completely new fields. This equipment has become increasingly popular for various applications [1]. Due to the ability to equip the UAV with multiple transmitters, sensors, photography equipment, herbicide spraying boom and various mechanisms for performing tasks, UAVs can be used in a wide range of applications. Success stories have been reported in areas, such as air reconnaissance [2], forest fire detection and extinguishing [3; 4], target observation [5], traffic monitoring and management [6], safety monitoring in constructions [7; 8], photogrammetry and three-dimensional mapping [9], determining the vegetation status of crops [10].

The finite element method is very common in design, because it allows simulation of processes [11-14], stress distribution in the structure [15; 16], assemblies, subassemblies or equipment [17], which are then verified by simulated and accelerated tests [18] to be validated in real conditions. Drop test studies evaluate the effect of the impact of a part or an assembly with a rigid or flexible planar surface. Dropping an object on the floor is a typical application, hence the name. The program calculates impact and gravity loads automatically. No other loads or restraints are allowed. Drop tests have been studied, but in other areas, not in the analysis of the framework of a UAV. Drop tests are for studying falling of different fruits and vegetables [19; 20], for different objects like test boards, pen drive, air conditioner, cartridge and dishwasher [21-25], or other studies of drop tests in the field of aviation, but not UAVs [26; 27].

The Drop Test Setup allows two calculation models:

- the first method is done by entering the height (h), the gravitational acceleration (g) and the impact plane in the calculation program. It will calculate the impact speed with the formula $v = (2 \cdot g \cdot h)^{1/2}$. The studied body will move in the same direction with gravity as a rigid body until it meets the rigid plane.
- the second method is done by entering the impact speed (v), the gravitational acceleration (g) and the impact plane, and then the program will determine the impact region based on the speed direction.

In principle, the system uses the energy conservation theorem (energy is not lost, it is only transformed), in which:

$$E_p = m \cdot g \cdot h = E_c = (m \cdot v^2)/2$$

where E_p – potential energy, J;
m – mass of the body subjected to analysis, kg;

g – gravitational acceleration, $m \cdot s^{-2}$;
h – height from which the body will fall, m;
E_c – kinetic energy, J;
v – body speed on impact, $m \cdot s^{-1}$.

The program solves a dynamic problem as a function of time. The general equation of motion is:

$$F_I(t) + F_D(t) + F_E(t) = R(t)$$

where $F_I(t)$ – inertia forces;
$F_D(t)$ – damping forces;
$F_E(t)$ – elastic forces.

All of these forces are time-dependent. In static analysis this equation is reduced to: $F_E(t) = R(t)$, since the inertia and damping forces are neglected due to small speeds and accelerations.

Materials and methods

The first stage is to transform and simplify the CAD model (a commercially UAV model AGRAS T-16, manufactured by DJI, after it was purchased, it was measured, and the frame reconstructed in Solidwokrs) and transform it into the CAE model (Fig.1) that can be introduced in the simulation. The most important assembly in a drone is the frame on which it lands, because it is most difficult to replace and will be the most requested part of the execution of a UAV, because most of the time it will land on it. The drop test was performed on the UAV depending on different angles of fall, namely, at 0º, 30º, 45º and 90º. Three simulations were performed, from a height of 4 m, which would be the working height in most situations, because it is a UAV used to apply plant protection products (Fig. 2). For a more detailed verification of the resistance, three additional analyses were performed from different heights of 10, 50 and 100 m.

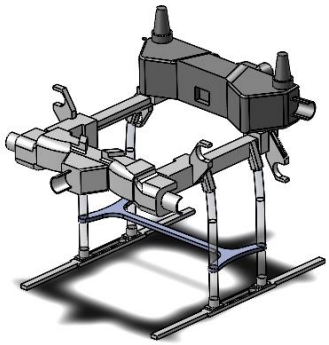

Fig. 1. **Simplified model for introduction in drop test simulation**

Fig. 2. **UAV for application of plant protection products (DJI AGRAS T-16)**

After the model has been simplified, the material was chosen, as most of the UAVs are made of different plastic composites. We chose to simulate the material polybutylene terephthalate (PBT), which is a semi-crystalline engineering thermoplastic material. It has similar properties and composition to polyethylene terephthalate (PET). It is a member of polyester family of polymers. Its properties are presented in Table 1.

Table 1

Properties of polybutylene terephthalate material

Tensile strength	$5.65 \cdot 10^7$ N·m^{-2}
Elastic modulus	$1.93 \cdot 10^9$ N·m^{-2}
Poisson's ratio	0.3902
Mass density	1300 kg·m^{-3}
Shear modulus	$6.902 \cdot 10^8$ N·m^{-2}

To enter the input data, we used the second method, in which we entered the height from which the assembly falls to check if it calculates the speed correctly using the formula $v = (2 \cdot g \cdot h)^{1/2}$.

The data entry was performed at setup by introducing the height of 4 m, the plane on which it will fall was set, in the first phase the drone falling straight, namely, at an angle of 0º, then at an angle of 30º, 45º and 90º, according to Figure 3.

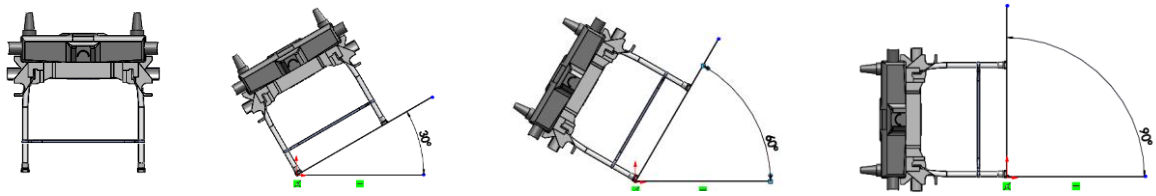

a) 0º, b) 30º, c) 60º, d) 90º

Fig. 3. **Positioning the drone at different angles**

After entering the input data, including the maximum time after impact to obtain the results, this time has been set to 30 microseconds, the CAE mode was discretized. The process starts with the creation of a geometric model. Then, the program subdivides the model into small pieces of simple shapes (elements) connected at common points (nodes), the settings being made in the create mesh command. Finite element analysis programs look at the model as a network of discrete interconnected elements. Standard solid type mesh was used, with 4.4388 mm element size and with a tolerance of 0.22194 mm, which resulted in a total number of 759075 elements and 143212 nodes. After creating the mesh, certain nodes were chosen after the first test simulation (Fig.4), where it seemed critical to measure the von Mises stress for each drop test performed.

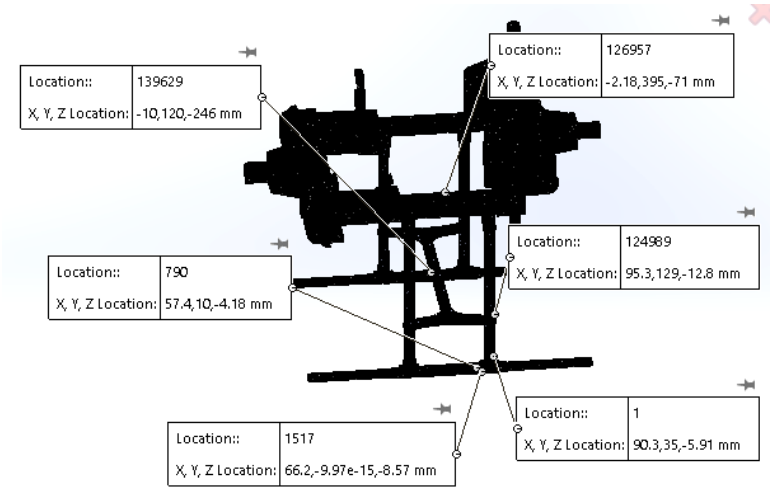

Fig. 4. **Positioning nodes selected for display of measurement results**

Results and discussion

The measured results were represented by equivalent stress distribution (von Mises Stress), distribution of the values of the relative resultant displacement field (resultant displacement) and distribution of total specific deformation field (equivalent strain). These results are presented using images and diagram charts, shown in Figure 5, only for the first simulation, drop test performed from 4 m with the fall at an angle of 0 º, the rest of the results being presented in Table 2.

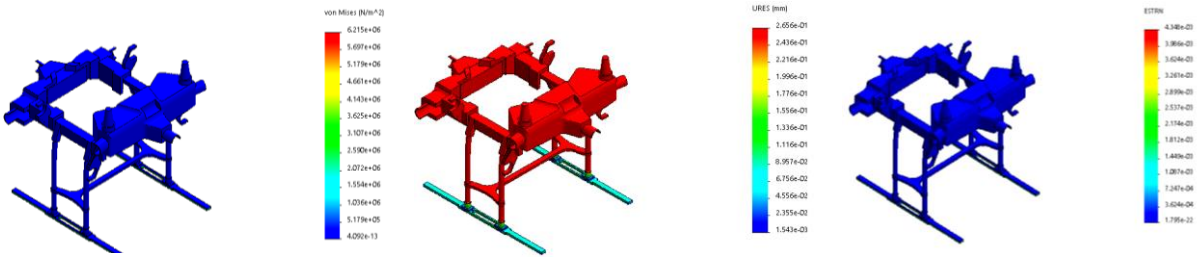

a) VON: von Mises Stress b) URES: Resultant Displacement c) ESTRN: Equivalent Strain

Fig. 5. **Representation for drop test at height of 4 m, with the fall angle at 0º**

Table 2

Maximum values (Resultant displacement, Equivalent strain) obtained for all simulations

Input data			Max. resultant displacement, mm	Max. equivalent strain
0	**Angle**	**Speed at impact, m·s^{-1}**		
4	0º	8.85	$2.652 \cdot 10^{-1}$	$4.348 \cdot 10^{-3}$
4	30º	8.85	$2.688 \cdot 10^{-1}$	$3.611 \cdot 10^{-3}$
4	60º	8.85	$3.185 \cdot 10^{-1}$	$3.601 \cdot 10^{-3}$
4	90º	8.85	$2.659 \cdot 10^{-1}$	$3.502 \cdot 10^{-3}$
10	0º	14	$4.200 \cdot 10^{-1}$	$2.886 \cdot 10^{-3}$
50	0º	31.32	$9.391 \cdot 10^{-1}$	$1.548 \cdot 10^{-2}$
100	0º	44.29	$6.215 \cdot 10^{6}$	$6.215 \cdot 10^{6}$

Equivalent stress distribution depending on the time appearing in the nodes in Figure 4 are represented graphically in Figure 6.

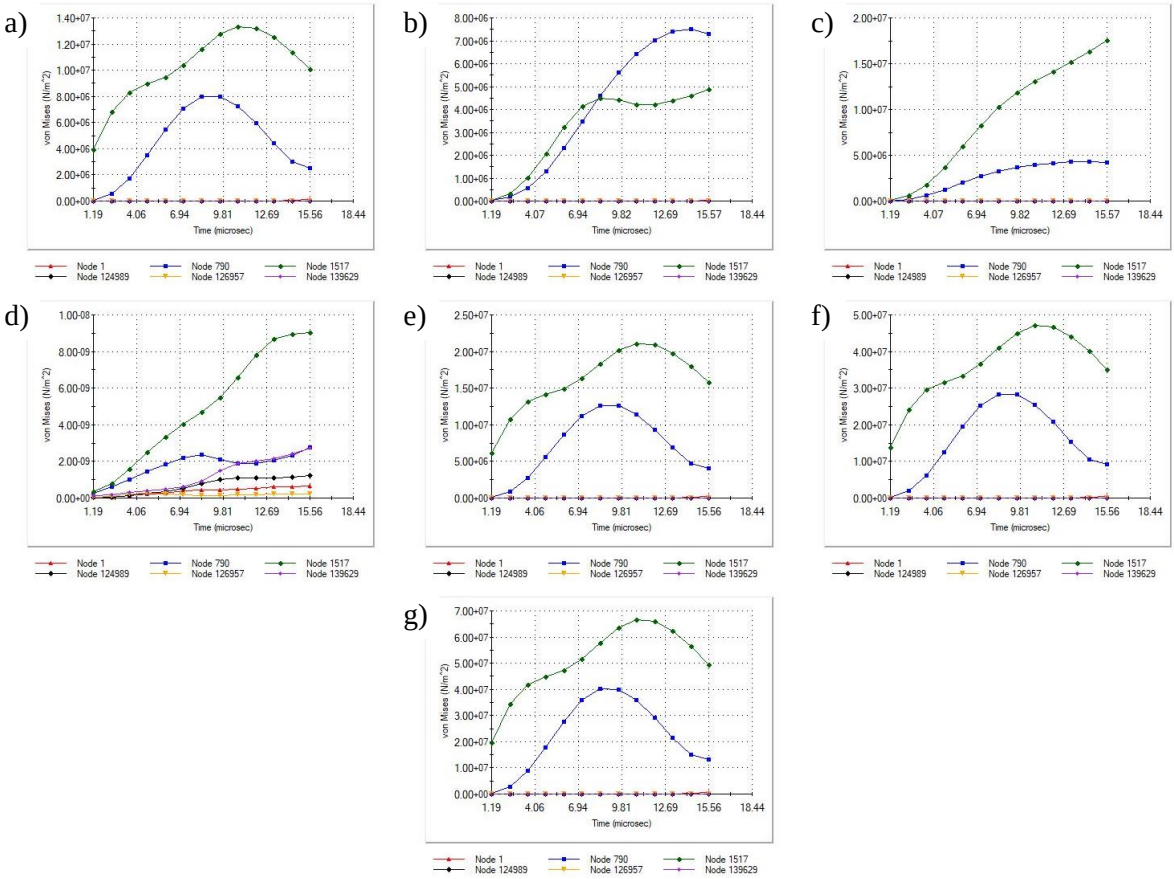

Fig. 6. **Equivalent stress distribution as a function of time appearing in the nodes from Fig. 4 for all simulations performed:** a – 4 m, 0º, 8.85 m·s^{-1}; b – 4 m, 30º, 8.85 m·s^{-1}; c – 4 m, 60º, 8.85 m·s^{-1}; d – 4 m, 90º, 8.85 m·s^{-1}; e – 10 m, 0º, 14 m·s^{-1}; f – 50 m, 0º, 31.32 m·s^{-1}; g – 100 m, 0º, 44.29 m·s^{-1}

Figure 6 shows the variation of equivalent stress in time in the nodes presented Figure 4, it can be seen that the highest equivalent stress occurs in the node 1517 and after that in the node 790, which are the nodes at the bottom of Figure 4, at the contact surface between the UAV and the ground. Only for the angle of 90 degrees can be seen an increase of the equivalent stress in the structure at the top, because direct contact occurs of the top structure with the ground.

Conclusions

1. The resulting displacements in the structure and equivalent strain increase potentially directly with the fall angle of the UAV, because the contact surface between the UAV and the rigid plane is not made on both landing bars and due to the change of the centre of gravity of the UAV, but at 90º it returns to a resulting displacement approximately equal to the value measured at 0º, because the top comes in contact with the surface.
2. Equivalent stress distribution up to a height of 50 m does not reach the tensile strength of the material $5.65 \cdot 10^7$ $N \cdot m^{-2}$, the highest value being $4.8 \cdot 10^7$ $N \cdot m^{-2}$, being so close to the value of material tensile strength. An analysis was performed at 100 m, where it was observed that the value recorded in node 1517 exceeds the tensile strength.
3. In conclusion, for a UAV made of PBT, at a fall from a height of more than 50 m, there will be consequences in the structure, so in the future measures it will be taken to strengthen the structure, modify the material or reduce the transported weight.

Acknowledgements

This work was supported by a grant of the Romanian Ministry of Education and Research, project code PN 19 10 02 01 – DEVELOPMENT OF INNOVATIVE TECHNOLOGIES IN SMART FARMS, contract no. 5N/07.02.2019, within the Program NUCLEU 2019 – 2022.

References

[1] Tsourdos A., White B. Shanmugavel M. Cooperative Path Planning of Unmanned Aerial Vehicles; John Wiley & Sons: Hoboken, NJ, USA, 2010.
[2] Sauerbier M., Siegrist E., Eisenbeiss H., Demir N. The practical application of UAV-based photogrammetry under economic aspects, ISPRS – International Archives of the Photogrammetry Remote Sensing and Spatial Information Sciences XXXVIII, 2012, pp. 45-50.
[3] Zharikova M., Sherstjuk V., Sokol I., Forest Fire-Fighting Monitoring System Based on UAV Team and Remote Sensing, EEE 38th International Conference on Electronics and Nanotechnology (ELNANO) At: Kyiv, Ukraine, 2018, pp. 663-668
[4] Pathak A., Esho A.A., Munna A.R., Chowdhury T., Tasin A.H. A smart semi-autonomous fire extinguish quadcopter: future of Bangladesh, International Journal of Advanced Research, 2020, pp. 1-15
[5] Rabah M., Rohan A., Talha M., Nam K.-H., Kim S.H. Autonomous Vision-based Target Detection and Safe Landing for UAV, International Journal of Control, Automation and Systems (2018), pp. 3013-3025.
[6] Kanistras K., Martins G., Rutherford M.J., Valavanis K.P. A survey of unmanned aerial vehicles (UAVs) for traffic monitoring, 2013 International Conference on Unmanned Aircraft Systems.
[7] Alizadehsalehi S., Yitmen I., Celik T., Arditi D. The effectiveness of an integrated BIM/UAV model in managing safety on construction sites, International journal of occupational safety and ergonomics: JOSE, 2018, pp. 829-844
[8] Anwar N., Najam F., Izhar M.A. Construction Monitoring and Reporting using Drones and Unmanned Aerial Vehicles (UAV's), The Tenth International Conference on Construction in the 21st Century (CITC-10), July 2-4, 2018, At: Colombo, Srilanka
[9] Muliady M., Sartika E.M., Lesmana C., Wianto E. UAV photogrammetry for generating 3D campus model, The 4th international conference on industrial, mechanical, electrical, and chemical engineering, 2019
[10] Găgeanu I., Cujbescu D., Matache M., Persu C., Voicea I., Vlăduț V., Oprescu R., Iuga D., Chiriță A.P., Duță D.E., Method for determining the vegetation state of crops through aerial mapping using an agricultural drone, International Sysmposium ISB-INMA TEH'2018, pp.265-270.

[11] Biriş S.Șt., Vlăduţ V. - Use of finite element method to determine the influence of land vehicles traffic on artificial soil compaction, WATER STRESS, pp. 179-198;
[12] Biriş S., Maican E., Faur N., Vlăduţ V., Bungescu S. - Fem model for appreciation of soil compaction under the action of tractors and agricultural machines, PROCEEDINGS OF THE 35 INTERNATIONAL SYMPOSIUM ON AGRICULTURAL ENGINEERING "Actual Tasks on Agricultural Engineering", pp. 271-280, 2007, Opatija – Croaţia;
[13] Ungureanu N., Vlăduţ V., Biriş S. - FEM modelling of soil behaviour under compressive loads, International Conference on Applied Sciences (ICAS2016), Hunedoara, Romania, 2016, Materials Science and Engineering, Vol 163(2017), 012001, pp. 1-9, doi:10.1088/1757-899X/163/1/012001;
[14] Ungureanu N., Vlăduţ V., Biriș S.-Ș., Paraschiv G., Dincă M., Zăbavă B. Ș., Ștefan V., Gheorghiță N. E. - FEM modelling of machinery induced compaction for the sustainable use of agricultural sandy soils, PROCEEDINGS OF THE 46 INTERNATIONAL SYMPOSIUM ON AGRICULTURAL ENGINEERING "Actual Tasks on Agricultural Engineering", pp. 201-211
[15] Biriş S., Maican E., Ungureanu N., Vlăduţ V., Murad E. - Analysis of stress and strain distribution in an agricultural vehicle wheel using finite element method, PROCEEDINGS OF THE 39 INTERNATIONAL SYMPOSIUM ON AGRICULTURAL ENGINEERING "Actual Tasks on Agricultural Engineering", pp. 107-118, 2011, Opatija - Croaţia;
[16] Biriş S., Vlăduţ V., Faur N., Cernescu A., Kabaş O., Matache M., Voicea I., Bungescu S., Popescu C - FEM analysis/testing resistance of a tractor seat, PROCEEDINGS OF THE 43 INTERNATIONAL SYMPOSIUM ON AGRICULTURAL ENGINEERING "Actual Tasks on Agricultural Engineering", pag. 189-200, 2015, Opatija - Croaţia
[17] Vlăduţ D.I., Biriş S., Vlăduţ V., Cujbescu D., Ungureanu N., Găgeanu I. – Verification of stress by FEM analysis·m^{-1}echanical testing of agricultural mobile aggregates couplig device, INMATEH – AGRICULTURAL ENGINEERING, vol. 54, no. 1/2018, pag. 37-46;
[18] Vlăduţ V., Gângu V., Pirnă I., Băjenaru S., Biriş S., Bungescu S. - Complex tests of the resistance structures in simulated and accelerated regime on hydropulse installation, PROCEEDINGS OF THE 35 INTERNATIONAL SYMPOSIUM ON AGRICULTURAL ENGINEERING "Actual Tasks on Agricultural Engineering", pag 393÷404, 2007, ISSN 1333-2651, Opatija – Croaţia;
[19] Kabaş O., Celik H.K., Ozmerzi A., Akinci I. Drop test simulation of a sample tomato with finite element, Journal of the Science of Food and Agriculture, Volume 88, Issue 9, 2008, pp. 1537-1541.
[20] Kabas O., Vladut V. Determination of Drop-Test Behavior of a Sample Peach Using Finite Element Method, International Journal of Food Properties, 18:11, 2015, pp. 2584-2592.
[21] Yeh M.-K., Huang T.-H. Drop Test and Finite Element Analysis of Test Board, Procedia Engineering, Volume 79, 2014, pp. 238-243;
[22] Imran M., Chandan M., Bharath B. S., Yeshawanth S. Drop test simulation on pen drive by using ansys, International Journal of Research in Engineering and Technology, Volume 4, 2015, pp. 240-245.
[23] Yayala P., Fazlı Teknec M. Failure Analysis of a Drop Tested Wall-Mounted Air Conditioner Indoor Unit: Simulation and Experimental Analysis, Journal of Science, 2020, pp. 843-855.
[24] Todorov G., Kamberov K. "Virtual prototyping of drop test using explicit analysis", AIP Conference Proceedings 1910, 020013 (2017) DOI: 10.1063/1.5013950
[25] Mulkoglu O., Guler M.A., Demirbag H. Drop Test Simulation and Verification of a Dishwasher Mechanical Structure, 10th European LS-DYNA Conference 2015, Würzburg, Germany;
[26] Gransden D., Alderliesten R., Benedictus R. Development of FEM Model for Comparing Metal and Composite Fuselage Section Drop Testing, ICRASH 2014;
[27] Hidayat D., Istiyanto J., Sumarsono D.A. Comparison Virtual Landing Gear Drop Test for Commuter Aircraft Utilize MSC ADAMS And Solidworks Motion Analysis, Journal of Physics: Conference Series, 5th International Seminar on Aerospace Science and Technology, Volume 1005, 2017.